Langmuir

Article

pubs.acs.org/Langmuir

Plasma-Enhanced Copolymerization of Amino Acid and Synthetic Monomers

Kyle D. Anderson,[†] Seth L. Young,[†] Hao Jiang,[‡] Rachel Jakubiak,[‡] Timothy J. Bunning,[‡] Rajesh R. Naik,[‡] and Vladimir V. Tsukruk*,[†]

[†]School of Materials Science and Engineering, Georgia Institute of Technology, Atlanta, Georgia 30332, United States

[‡]Materials and Manufacturing Directorate, Air Force Research Laboratory, Wright-Patterson Air Force Base, Dayton, Ohio 45433-7702, United States

ABSTRACT: In this paper we report the use of plasma-enhanced chemical vapor deposition (PECVD) for the simultaneous deposition and copolymerization of an amino acid with other organic and inorganic monomers. We investigate the fundamental effects of plasma-enhanced copolymerization on different material chemistries in stable ultrathin coatings of mixed composition with an amino acid component. This study serves to determine the feasibility of a direct, facile method for integrating biocompatible/active materials into robust polymerized coatings with the ability to plasma copolymerize a biological molecule (L-tyrosine) with different synthetic materials in a dry, one-step process to form ultrathin coatings of mixed composition. This process may lead to a method of interfacing biologic systems with synthetic materials as a way to enhance the biomaterial−tissue interface and preserve biological activity within composite films.

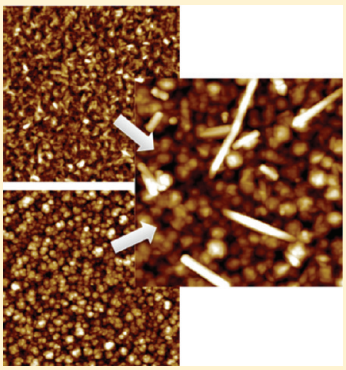

INTRODUCTION

Chemical vapor deposition (CVD) methods have been widely used to polymerize materials directly on a variety of surfaces.[1−4] CVD processes have been designed to allow organic monomers to undergo in situ polymerization during the deposition process, resulting in a stable film of polymerized material on the surface. Polymerization is initiated by a range of different stimuli, including radio frequency (rf) plasma radicalization, oxidation, and injection of an initiator into the reaction chamber.[5−12] Each deposition method has the effect of creating a polymerized film on a target substrate with different variations in the cross-linking density and morphology depending on the CVD method used and the reaction mechanisms.[13] This leads to films with a wide range of unique surface properties that can be tailored for many specialized applications.

Plasma-enhanced chemical vapor deposition (PECVD) is a specific form of CVD which has been adapted from its common use to deposit dielectrics to successfully deposit a wide range of monomers covering many traditional polymers, ranging from styrene, acrylonitrile, and benzene to responsive materials such as poly(2-vinylpyridine) and poly(*N*-isopropylacrylamide) to functional amino acids.[14−22] PECVD represents a versatile "dry" chemistry fabrication method which is capable of utilizing precursors in solid, liquid, or gas form for facile, rapid, and solvent-free fabrication of ultrathin coatings for use in many systems.[23−26] There is a growing interest in the deposition of biological molecules via PECVD, which can potentially be used to enhance surface functionalities and structures for cell viability and can also help to bridge the interface between inorganic and biologic components of integrated systems and biomedical applications.[3,27−31]

Biological monomers of interest are oftentimes in the form of a powdery solid, presenting a unique set of challenges for plasma depositions of these monomers. Some solid monomers can be deposited through various sublimation methods whereby the monomers are preheated in the plasma chamber while under vacuum and vaporized into a gas phase.[32−36] The reaction proceeds akin to any gas-phase monomer. It has been demonstrated that sublimation PECVD is compatible with a range of materials, from organometallics to amino acids, providing robust and stable films.[18,19,32,33] The utilization of sublimation allows solid materials which are not easily vaporized to be plasma deposited, opening a new range of solid material precursors for study.

Amino acids might be deposited via sublimation PECVD and are excellent candidates for further investigation on the basis of their unique functionalities and fundamental biologic characteristics.[18,19,37,38] In a recent study, Lee and Frank demonstrated vapor deposition of a wide range of amino acids which were firmly grafted to a substrate and preserved their composition and functionalities.[30] PECVD lends itself well to copolymerizations of two or more chemical species to facilitate complex and stable functionalized mixed coatings. However, this adds a layer of complexity to the deposition process given the different reactivities of the precursors used. For instance, copolymerization has been previously reported using benzene and octafluorocyclobutane (liquid and gaseous) monomers which

Received: November 9, 2011
Revised: December 11, 2011
Published: December 16, 2011

are copolymerized in the plasma simultaneously to fabricate films with controllable refractive indices.[39]

One challenge with this fabrication process though is determining the appropriate deposition conditions which allow a controlled reaction of different organic materials simultaneously. This challenge is magnified when using one monomer which is solid and must be sublimed into the plasma stream since flow rates are not as easily controlled as they are with conventional liquid- and gas-phase monomers. In this regard the deposition rates of each material must be matched on the basis of the desired end ratio of the final film composition. As the monomers are mixed in the plasma stream, they form highly randomized structures which when deposited exhibit characteristics of both components.[39,40] Despite the utility of the sublimation PECVD procedure of biological molecules, examples of robust and uniform binary plasma-polymerized films utilizing them are very rare. Developing the capability of simultaneous depositions with different monomers, including bioactive compounds, of any important material highlights the versatility offered to the composition of the resulting plasma-polymerized films.

In this study, we demonstrate the PECVD copolymerization of the sublimed amino acid (L-tyrosine) with vaporized liquid monomers, which results in stable and uniform ultrathin coatings with unique surface morphologies and characteristics. PECVD copolymerization of L-tyrosine (Tyr) was carried out with several different monomers such as acrylonitrile, (ACN), 2-hydroxyethyl methacrylate (HEMA), and titanium tetraisopropoxide (TTIP). The organic and inorganic functional monomers used were chosen to demonstrate the feasibility of the integration of an amino acid with other synthetic materials which have been extensively studied to date. The amino acid L-tyrosine was chosen for this study due to important bioactive function in peptides, the expected compatibility with sublimation PECVD, and the well-understood plasma deposition parameters.[18,37] It is hoped that L-tyrosine provides insight into the copolymerization of biologic molecules with other materials for many biointerfacial applications.[3] A single amino acid is used in this study with the intention of further expanding the forthcoming study to other amino acids and eventually longer sequence peptide chains.

ACN was utilized due to its compatibility with our plasma deposition process. Many previous studies have evaluated this polymer and its deposition characteristics.[9,41,42] This fact allowed the focus of this deposition to be centered on controlling the tyrosine deposition rate for proper material mixing in the plasma. HEMA is an example of a material which has been previously characterized and demonstrated as biologically compatible with its use in implants.[43,44] Previous studies have further characterized CVD HEMA as a swellable material.[16,17,45,46] Any future integration of biological materials to form composite films must include a second component which has been well characterized and is understood to be biologically compatible, such as HEMA.[47]

In this study HEMA serves as a biocompatible material for copolymerization as it has been previously combined with tyrosine through radicalization via peroxide and UV polymerization.[48] Finally, titanium tetraisopropoxide was used since it provides a facile method of introducing an inorganic component to the amino acid films. Creating such an interface on the nano- to microscale in this manner makes it a potentially useful interface, which more easily allows the integration of implants with biological systems. The different materials selected here were simultaneously reacted during the plasma deposition to (a) determine their ability to form ultrathin stable, robust, uniform coatings with chemically mixed composition and (b) determine the copolymerization characteristics of biologic molecules with organic and inorganic materials for fabrication of bioactive plasma-polymerized coatings.

EXPERIMENTAL SECTION

Materials. All monomers, L-tyrosine (98%), acrylonitrile (99%), 2-hydroxyethyl methacrylate (97%), and titanium tetraisopropoxide (97%) were purchased from Sigma-Aldrich and used as received for all plasma processes described (Scheme 1). All depositions were carried out on highly polished single-crystal {100} silicon wafer substrates (University Wafer) cleaned in piranha solution (3:1 concentrated H_2SO_4 and 30% H_2O_2) and rinsed with Nanopure water (18 MΩ cm) according to the accepted procedure.[49]

Scheme 1. Chemical Structures of the Compounds Studied and Diagram of the Sublimation PECVD Chamber Setup for Copolymerization with an Inlet for Additional Monomers Showing Flow of Monomers to the Surface in a Random Configuration[a]

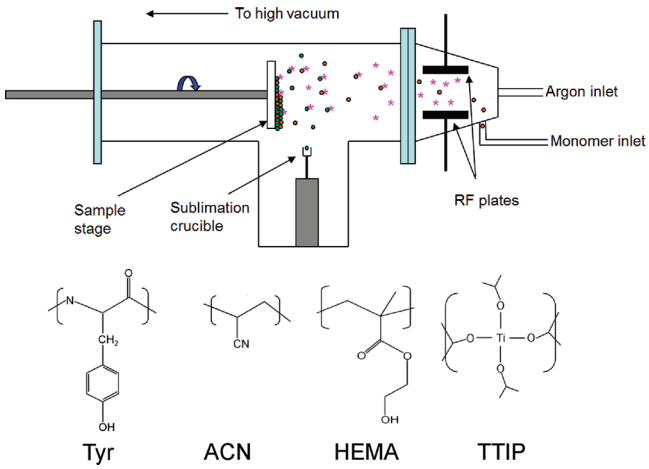

[a]Circles represent monomers in the PECVD chamber, while stars represent radicals.

All plasma reactions and depositions were carried out in a custom-built flowing afterglow plasma chamber which utilized a capacitively coupled rf power source (13.56 MHz) for plasma generation in a low-pressure argon atmosphere.[32,50,51] The sublimation of tyrosine in the PECVD chamber was run according to the established procedure and utilized both downstream and plasma zone monomer inlets, where the sublimation boat was placed downstream of the plasma-generating zone.[18,52,53] The specific configuration used in this study utilized the modified sublimation chamber with a heating crucible and an end cap containing a second inlet for the liquid monomer delivery (Scheme 1).

The solid L-tyrosine monomer was placed in a resistively heated tantalum crucible and heated to approximately 200 °C to begin the sublimation and then subsequently reduced to approximately 140 °C after sublimation had begun and held at this temperature for the remainder of the deposition. The monomers deposited in liquid form (ACN, HEMA, TTIP) were placed in a custom-built vaporizing tube connected to the reaction chamber and heated to 60 °C in a water bath. The lines running from the vaporizing tube to the chamber were also heated to 60 °C to prevent condensation of the monomer in the tubes. The depositions of tyrosine, ACN, HEMA, and all associated copolymerizations were run under varying sets of conditions which were in the ranges listed: 20−45 W power, 0.05−0.1 Torr operating pressure, 20−50 sccm Ar carrier gas flow rate, and 6−12 min

dx.doi.org/10.1021/la204416h | Langmuir 2012, 28, 1833−1845

deposition time. The variation in conditions allowed for control of the cross-linking density of the film.[54] The TTIP depositions were run under identical conditions with the addition of an oxygen carrier gas at 20−50 sccm instead of argon. This was used for both the pure PP-TTIP and PP-Tyr/TTIP films. After the plasma-enhanced deposition, the films were removed from the chamber and allowed to rest for a minimum of 48 h before further modification or analysis to allow all internal stresses to equilibrate.

Characterization. Atomic force microscopy (AFM) images were collected using an Icon AFM microscope with a Nanoscope V controller (Bruker) under the quantitative nanomechanical mapping (QNM) regime in air.[55] Triangle ScanAsyst-Air cantilevers (Bruker) with a nominal spring constant of 0.4 N m^{-1} were used for all measurements. Scan sizes from 20 μm to 500 nm were collected at an optimized scan rate of 1 Hz. The surface distribution of relative mechanical properties was collected in the peak-force mode, and the Derjaguin−Müller−Toropov (DMT) model was used to calculate the elastic modulus.[56,57] All surface (rms) microroughness measurements were conducted over six 1 × 1 μm^2 area and averaged over several surface locations.

Surface compositions were obtained with X-ray photoelectron spectroscopy (XPS) using a Thermo K-Alpha XPS system with an Al Kα source and utilizing charge neutralization. The initial spectra were collected over the range of 0−1300 at 1 eV steps with a spot size of 300 μm averaged over two scans. High-resolution scans were performed in the range of relevance for specific elements at 0.1 eV steps and averaged over five scans. Energy-dispersive spectroscopy (EDS) was performed with an Oxford system on a Hitachi S-3400 scanning electron microscope.

Fourier transform infrared (FTIR) spectroscopy measurements were conducted using a Bruker FTIR spectrometer (Vertex 70) equipped with a narrow-band mercury cadmium telluride detector in reflection mode.[58] Spectra were collected from 4000 to 500 cm^{-1} at 1 cm^{-1} resolution, and 16 scans were averaged. All thickness and optical measurements were performed using an M-2000U variable-angle spectroscopic ellipsometer (Woollam Co.) with measurements at 65°, 70°, and 75° and a spectral range from 350 to 1000 nm. All modeling of ellipsometric data was done using a Cauchy model in accordance with the usual practice.[59] Contact angle measurements were collected using a KSV CAM 100 system and placing a 2 μL drop on the surface.

RESULTS AND DISCUSSION

Single-Material Depositions. Prior to beginning copolymerization PECVD experiments, each monomer was deposited and characterized independently to evaluate the quality of the ultrathin films formed. All monomers were deposited on clean silicon substrates and characterized by AFM to determine the morphology of the PECVD films and the mechanical stability of each coating. All films were deposited to a thickness of between 200 and 300 nm as measured by spectroscopic ellipsometry and were characterized with FTIR and XPS to determine the composition in addition to AFM. Significant differences were noted in the morphology among the four materials evaluated here.

AFM imaging shows the resulting depositions of all materials on clean silicon surfaces (Figures 1 and 2). The dry L-tyrosine (PP-Tyr) powder was sublimed for deposition (Figures 1A and 2A). The liquid acrylonitrile (PP-ACN) monomer was deposited by the standard vaporization method (Figures 1B and 2B), and the liquid HEMA (PP-HEMA) monomer was heated to 60 °C and deposited as a standard vapor deposition (Figures 1C and 2C). Large-scale AFM images show very uniform surface morphology of all films, indicating highly homogeneous composition with low surface microroughness, which is indicative of uniform cross-linking and wetting of the deposits of all components. These films are free of pinhole defects as well. This observation is in good agreement with

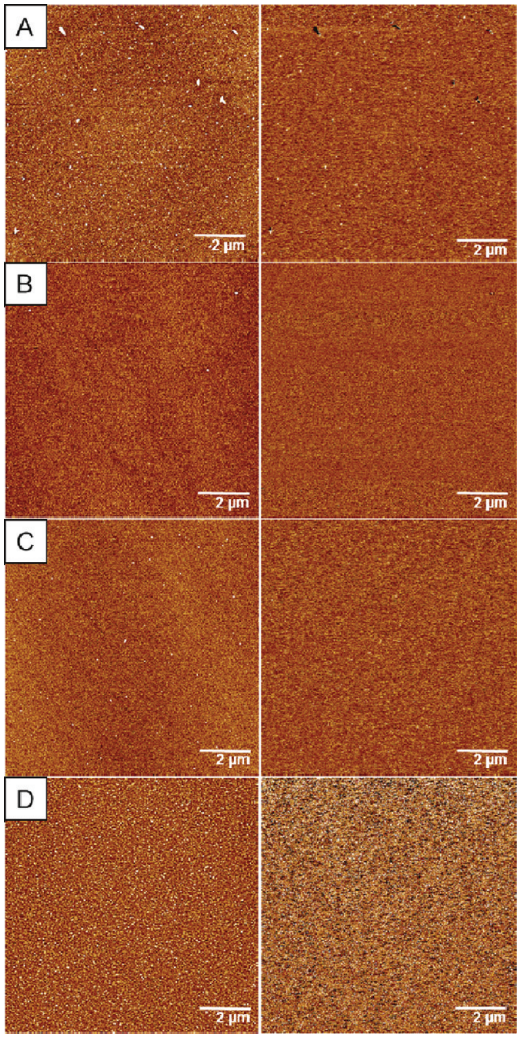

Figure 1. AFM images of (A) PP-Tyr, (B) PP-ACN, (C) PP-HEMA, and (D) PP-TTIP coatings. The left images show the topography (z(A,B,C) = 4 nm, z(D) = 24 nm), and the right images show the relative surface stiffness (arbitrary z scales).

previous studies of tyrosine and published literature regarding HEMA.[16,18] The surface microroughness of each sample was measured to be 0.6, 0.3, and 0.4 nm for PP-Tyr, PP-ACN, and PP-HEMA, respectively, which correspond to values usually reported for PECVD films in the literature for different materials.[60] These values correlate well with our previous data for microroughness for the various polymer and amino acid films obtained via PECVD.[18,41]

Corresponding high-magnification AFM images show the differences in the fine morphologies of the plasma-polymerized films of each coating (Figure 2). The PP-Tyr film shows a distinctive morphology composed of many small, distinct needle-like domain structures (~50−100 nm in length and diameter below 10 nm) which differs from the more uniform texture features of PP-ACN and PP-HEMA films where the dimensions of isolated round grains are within 20−50 nm. The PP-Tyr structure becomes clearly evident under the highest resolution scanning (300 nm × 300 nm), where it is observed that the domains are in fact individual tubular structures in random orientations on the surface (Figure 2A, right image). Three organic films show significant differences in morphology, structure, and roughness when compared to the much rougher

dx.doi.org/10.1021/la204416h | Langmuir 2012, 28, 1833−1845

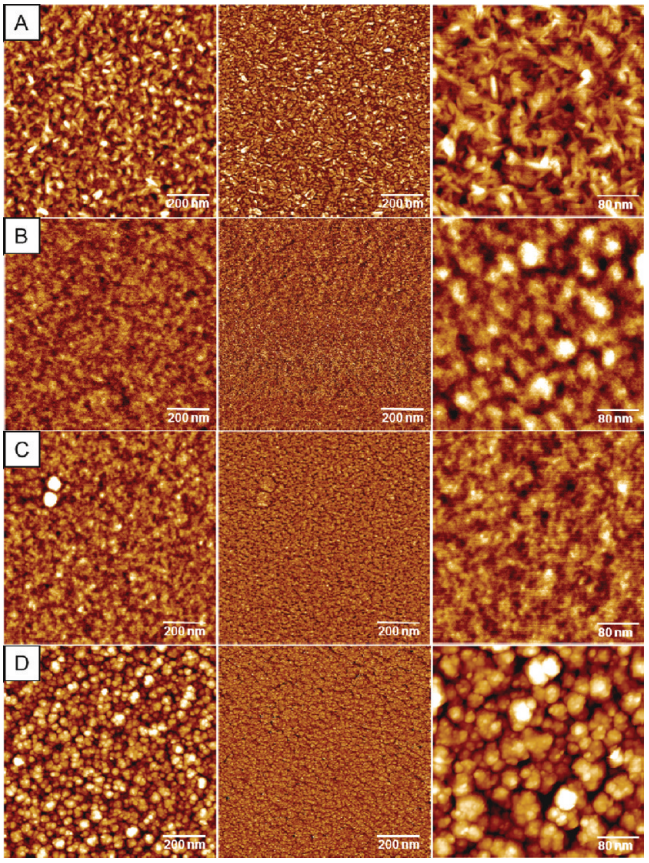

Figure 2. High-resolution AFM images of (A) PP-Tyr, (B) PP-ACN, (C) PP-HEMA, and (D) PP-TTIP coatings: (left) topography (z(A,B,C) = 4 nm, z(D) = 24 nm), (center) relative surface stiffness (arbitrary z scales), (right) high-resolution topography (z = 4 nm (A), 6 nm (B), 3 nm (C), and 24 nm (D)).

PP-TTIP inorganic coating. These distinctions in film morphology are important to note, as they govern properties such as microroughness and show that each material will deposit in a unique manner, even under similar deposition conditions.

The PP-TTIP film was deposited in an oxygen-rich atmosphere as a homogeneous film on a larger scale and showed a characteristically coarse grainy surface with a high porosity composed of aggregated and coarser features with cluster dimensions above 40 nm which are composed of 10−20 nm round grains (Figure 2D). Such morphology results from the plasma deposition in the presence of oxygen as previously reported.[61,62] According to previous studies, the resulting porous surface is a product of the deposition in an oxygen-rich environment in which the titanium atom of the TTIP will completely radicalize to a Ti^{4+} state. This is in contrast to the partial radicalization (Ti^{3+}) which occurs in a pure argon environment and is resistant to complete oxidation upon removal from the vacuum.[36,63,64] The surface microroughness of the pure titania film was measured at 3.6 nm, which is much larger than that measured for the organic and biological plasma-deposited films and larger than that of a PP-TTIP film deposited under an argon atmosphere. The oxygen-rich deposition was used as a method to promote the highest possible valence state of the titanium atom, allowing for an increased number of bonding sites for oxygen, which creates titania molecules with a 2:1 oxygen:titanium stoichiometry. In some instances, the introduction of oxygen may provide a nonideal deposition regime for the second material as oxidation can occur. However, it was observed that the resulting copolymerized films were stable when deposited with oxygen present in the chamber and were not significantly affected by this change in the atmosphere.

The AFM images of each of these materials show the topography and the relative surface stiffness distribution (in relative units) obtained from peak-force mode scanning (Figures 1 and 2).[65] In addition to a smooth topography, all coatings exhibit a uniform surface stiffness across the surface with very modest variation, indicating that there are no local surface regions of dramatically different mechanical properties, and thus, a uniform distribution in cross-linking density of the plasma-deposited films can be suggested. When compared to the traditional spin-cast films of the same materials (both monomer and polymer coatings), the plasma-deposited films were seen to be much more stable, have greater adhesion to substrates and were much more uniform, albeit ultrathin coatings.

Chemical Composition of Single-Material Films: FTIR Studies. The chemical composition of plasma-polymerized films was evaluated from FTIR spectra with several characteristic peaks detectable for each monomer (Scheme 1, Table 1, Figure 3). The PP-Tyr film shows key absorption peaks around 3200 cm^{-1}, which corresponds to the O−H stretch, and around

Table 1. Polymerized Films with the FTIR Peak Assignment

	PP-TYR	PP-ACN	PP-HEMA	PP-TTIP	PP-TYR/ACN	PP-TYR/HEMA	PP-TYR/TTIP
NH stretch		3270				3263	
OH stretch	3208		3283	3256	3204		3200
amine peak	3025				3024		
CH_2 asymmetric stretch		2940	2970		2962	2935	
CH_3 symmetric stretch			2873			2875	
C≡N stretch (cyano)		2215			2220		
C═O stretch			1723			1725	
C−C stretch	1610	1675	1640	1628	1611	1611	1612
C−C/C−H (ring)	1514				1515	1516	1515
CH_2 in-plane bending		1450	1459		1452	1456	1447
C−C stretch	1332			1344	1331	1330	1330
ring OH vibration	1257				1244	1247	1250
NH_2 backbone bending	829				840	839	857
Ti−O				696			697

dx.doi.org/10.1021/la204416h | Langmuir 2012, 28, 1833−1845

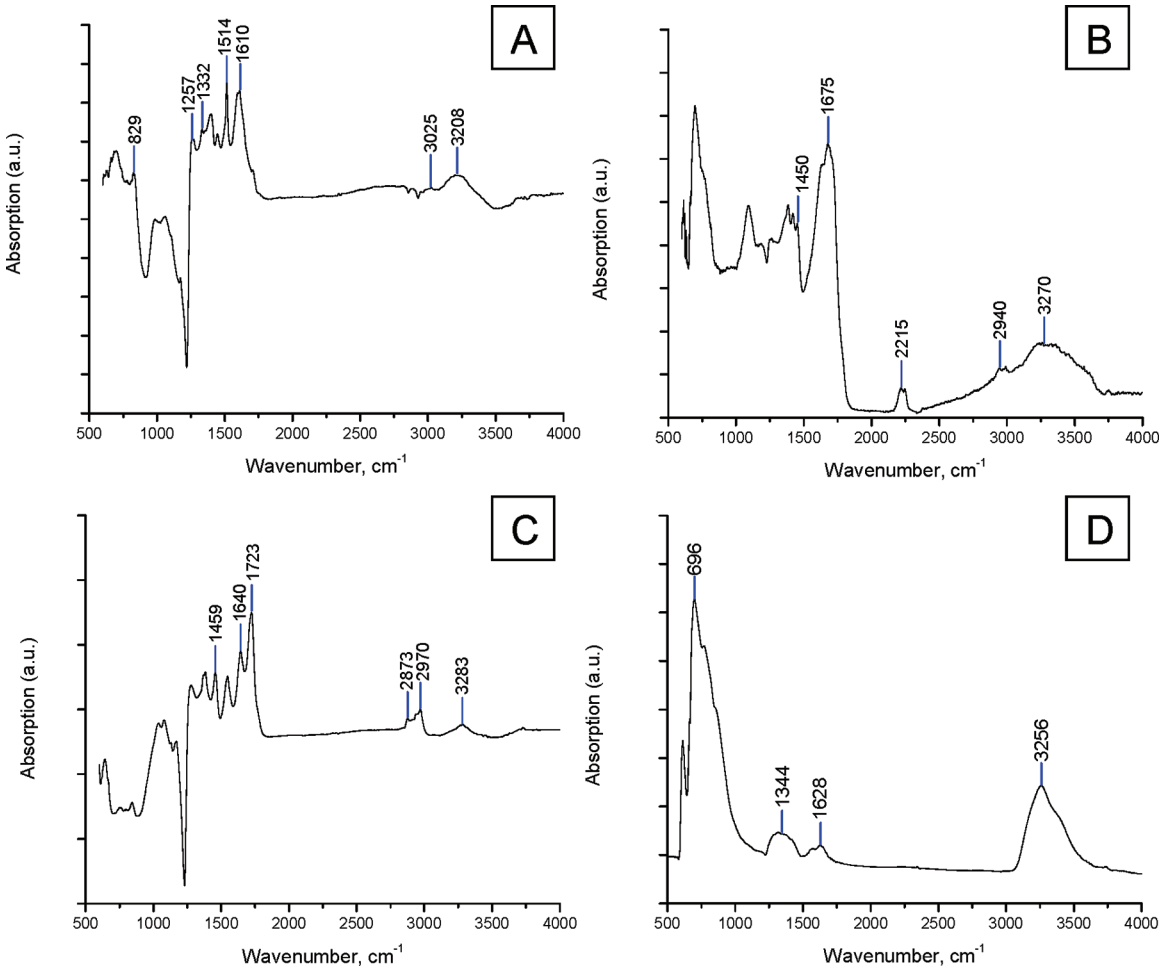

Figure 3. ATR-FITR (ATR = attenuated total reflection) spectra from coatings: (A) PP-Tyr, (B) PP-ACN, (C) PP-HEMA, (D) PP-TTIP.

3000 cm^{-1}, representing an amine peak (Figure 3A).[66] The preservation of the ring structure during plasma-assisted polymerization is confirmed by the presence of peaks at 1610, 1514, and 1332 cm^{-1} which correspond to the intact aromatic ring C−C double and single bond vibrations.[67] The peak seen at 1257 cm^{-1} confirms the presence of O−H groups attached to the aromatic ring. The NH_2 bending vibration peak occurring at 829 cm^{-1} in the PP-Tyr film has been previously observed to be a marker present in polytyrosine which shifts during cross-linking from an original position of 876 cm^{-1}.[18] This band is a key indicator of the cross-linking that is occurring in the film as it is deposited.

The FTIR spectrum for the PP-ACN film shows several intense peaks indicative of a high degree of cross-linking (Table 1, Figure 3B). The first is seen as a large, broad peak around 3270 cm^{-1} present from the N−H stretching, and the second is the C═N stretching mode seen around 1675 cm^{-1} along with the peak at 1092 cm^{-1} from C−N which results from the cyano group dissociation and cross-linking.[41] The observed peaks of CH_2 stretching at 2940 cm^{-1} and C−C stretching at 1450 cm^{-1} are also indicators of the preservation of backbones. The C≡N stretch seen around 2215 cm^{-1} is characteristic of the cyano group, indicating its presence in the plasma-deposited film.

The PP-HEMA spectra exhibit several characteristic peaks, including a broad O−H stretch around 3283 cm^{-1} and a C═O stretch at 1723 cm^{-1} (Figure 3C).[45] Both of these groups are seen in the side structure, and their presence indicates that they remained intact during the plasma deposition. Additional side chain peaks also seen are a CH_2 asymmetric stretch at 2970 cm^{-1}, a CH_3 symmetric stretching at 2873 cm^{-1}, CH_2 in-plane bending at 1459 cm^{-1}, and C−O−C asymmetric and symmetric stretching vibrations at 1079 and 1037 cm^{-1}. As indicated by Pfluger et al., the absence of a peak in the range of 3060−3010 cm^{-1} and at 1600 cm^{-1} indicates that no H—C═C structure is present in the PECVD film, indicating no residual monomer, as this double bond structure is not expected in a polymerized HEMA film. Also, the OH peak around 3300 cm^{-1} is expected to be minimized with higher cross-linking, which is the case in the sample measured, indicating that significant cross-linking is occurring in the PP-HEMA film.[46] This agreement of the measured PP-HEMA films with established literature values provides strong evidence of efficient polymerization occurring under given plasma deposition conditions.[16,68]

Finally, the PP-TTIP film exhibited a characteristic Ti−O peak near 700 cm^{-1} (Figure 3D). The peak seen is expected to contain minimal contributions from the silicon substrate as these peaks were carefully accounted for during the measurements and result primarily from the convolution of the Ti−O and residual carbon peaks, indicating polymerization reactions in accordance with known mechanisms.[69] In this case additional carbon peaks are seen at 1628 and 1344 cm^{-1} that correspond to the C═C and CH_3 bending vibrations, respectively.[63] The O−H stretching peak at 3256 cm^{-1} is also consistent with the predicted reaction products as well as a result of the silicon

dx.doi.org/10.1021/la204416h | *Langmuir* 2012, 28, 1833−1845

Table 2. Atomic Percentages of Key Elements from XPS Data

	theoretical composition				experimental results			
compound/composition	C	O	N	Ti	C1s	O1s	N1s	Ti2p
Tyr	59.6	26.5	7.7	0.0	68.5	21.8	9.7	0.0
ACN	67.8	0.0	26.4	0.0	71.0	13.5	12.8	0.0
HEMA	55.3	36.9	0.0	0.0	77.6	22.4	0.0	0.0
TTIP	50.7	22.5	0.0	16.9	34.1	48.2	2.0	15.9
composite films								
Tyr/ACN	61.5	20.5	12.0	0.0	69.6	21.2	7.5	0.0
Tyr/HEMA	57.8	30.8	4.5	0.0	75.4	21.6	3.0	0.0
Tyr/TTIP	54.1	24.1	3.0	10.3	69.2	22.9	6.8	0.0

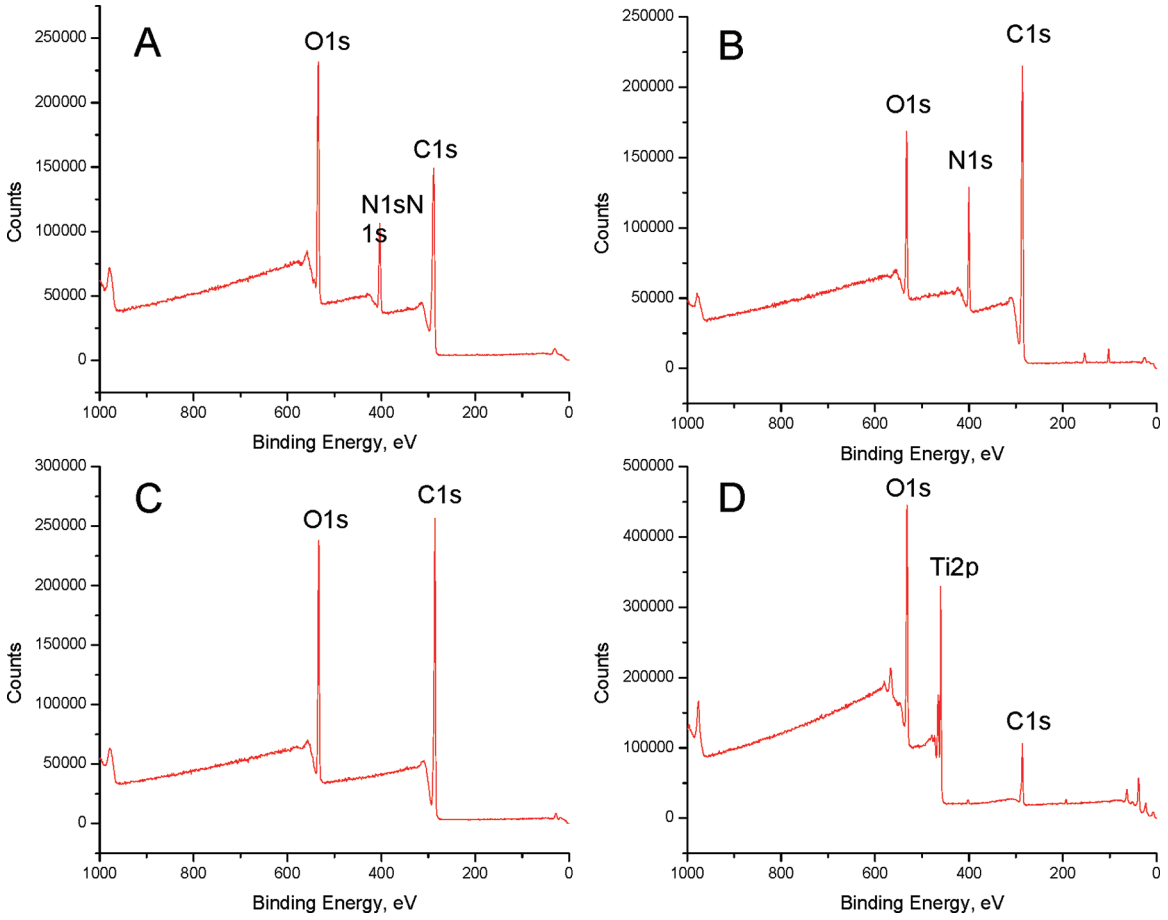

Figure 4. XPS plots for (A) PP-Tyr, (B) PP-ACN, (C) PP-HEMA, and (D) PP-TTIP coatings.

substrate used where surface hydroxylation occurs during the cleaning process. This spectrum confirms the presence of the titania as well as expected byproduct from the dissociation of the TTIP monomer during the plasma deposition.

Overall, the FTIR results discussed above confirm that the PECVD coatings contain key chemical features intact and are not structurally compromised. The data also indicate that chain formation and cross-linking are occurring among the monomers as they are deposited.

Chemical Composition of Single-Material Films: XPS Analysis. XPS analysis of the plasma-polymerized coatings confirms the expected compositions corresponding to their original chemical structures (Scheme 1, Table 2). PP-Tyr and PP-ACN showed the expected carbon, nitrogen, and oxygen peaks, whereas PP-HEMA shows only the carbon and oxygen peaks (Figure 4A–C, Table 2). The PP-TTIP film shows a strong Ti peak as well as significant oxygen with some residual carbon content in the film (Figure 4D). The residual carbon in the PP-TTIP film results from the number of methyl groups attached to the oxygen atoms which react to form a separate carbon system that is deposited on the surface as detailed elsewhere.[63]

The measured compositions generally correspond well to theoretically calculated ones on the basis of the chemical structures of the monomers (Table 2). This correlation indicates that the plasma-deposited films are maintaining roughly the same atomic composition of the monomers, except for a few cases, notably PP-HEMA, which shows an excess of carbon, likely resulting from surface carbon contamination upon exposure to air. Both the PP-TTIP films show less carbon and more oxygen than expected, which is likely due to the loss of carbon as a byproduct of the deposition, which is aimed at

dx.doi.org/10.1021/la204416h | Langmuir 2012, 28, 1833–1845

capturing the titanium and oxygen on the surface. Since this deposition was done in an oxygen-rich plasma, contributions to the oxygen content of the film could also be present from this source as well as absorption from the atmosphere, as is likely the case with PP-ACN.[64]

Copolymerizations of Different Compounds. The first copolymerization of L-tyrosine and ACN was carried out with simultaneous use of the sublimation apparatus and vapor bubbler to introduce both materials to the plasma reactor. Care was taken to match the deposition rates of the two materials to minimize nonuniformity of the mixed films deposited. Matching the deposition rates was done by first depositing PP-Tyr on a clean silicon wafer and measuring the thickness, giving a deposition rate calibration for a particular set of conditions. These conditions were then verified for compatibility with the second monomer, and an appropriate monomer flow rate for the second monomer was then calibrated so that the two monomers could be simultaneously deposited.

At a large scale, the resulting composite films from two different monomers are relatively smooth and defect free, showing relatively few features (Figure 5). There was an

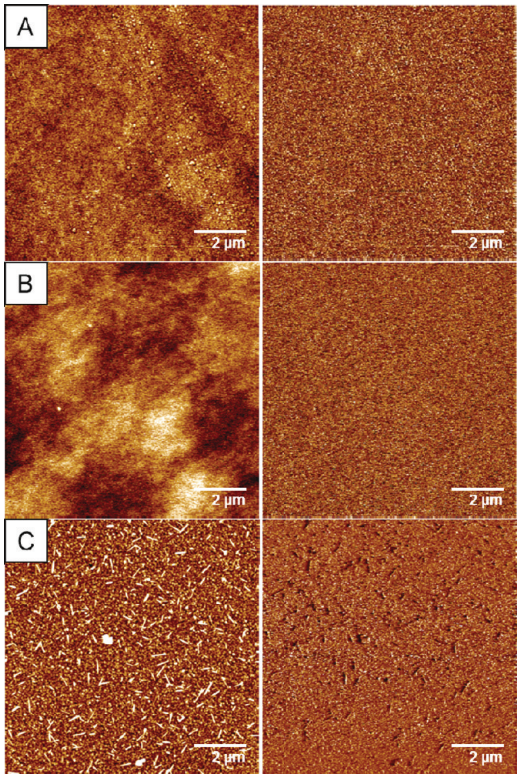

Figure 5. AFM images of copolymerized films: (A) PP-Tyr/ACN, (B) PP-Tyr/HEMA, (C) PP-Tyr/TTIP, (left) topographies A (z = 14 nm), B (z = 8 nm), and C (z = 24 nm), (right) surface stiffness (arbitrary z scales).

increase seen in the surface microroughness compared to that of the two single-material depositions. The microroughness was measured at 1.4 nm, which represents a 3-fold increase over that of the single-monomer films. Apparently, mixing two monomers results in the cross-linked network having regional variations and a grainy morphology, which increases the overall roughness of the film. The typical surface feature size ranges from 5 to 10 nm in height and from approximately 10 to 50 nm laterally, depending on the film composition. Overall the surface stiffness remains relatively uniform on a large scale, confirming the absence of microscopic dewetting and aggregation.

Next L-tyrosine and HEMA monomers were deposited onto the silicon surface simultaneously while under an argon atmosphere. The deposition rates of L-tyrosine and HEMA were matched so that the deposition occurred with a deposition rate of approximately 20 nm/min. Heating of the L-tyrosine monomer was begun prior to engagement of the plasma so that the material would be subliming as soon as the plasma was activated and HEMA introduced into the system. Both the ACN and the HEMA monomers deposited similarly to the L-tyrosine but produced dissimilar features in the final film.

An interesting and distinct microstructure was observed in the composite film that is not seen in either of the monomer films under high-resolution AFM imaging (Figure 6). The

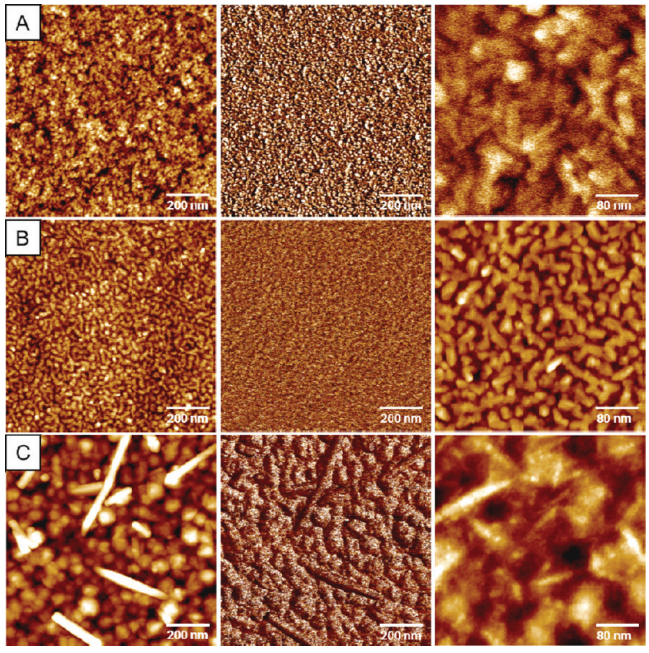

Figure 6. High-resolution AFM images of composite films: (A) PP-Tyr/ACN, (B) PP-Tyr/HEMA, (C) PP-Tyr/TTIP, (left) topographies A (z = 14 nm), B (z = 8 nm), and C (z = 24 nm), (center) surface stiffness (arbitrary z scales), (right) high-resolution topography (z = 8 nm (A), 8 nm (B), and 16 nm (C)).

surface stiffness distribution shows some inhomogeneities which are also seen in the topography. These variations of topographical features are measured to be less than 4 nm in height and are only clear at the highest magnifications. Moreover, the PP-Tyr/ACN film shows tubular-like structures very similar to those observed for the PP-Tyr film but in a much more diluted version. A distinctive morphology also seen in the PP-Tyr/HEMA film is reminiscent of the appearance of a microphase-separated system at the nanoscale. There is a distinct lack of tubular-like PP-Tyr morphological structures in the PP-Tyr/HEMA film that are seen in both PP-Tyr/TTIP and high-resolution PP-Tyr/ACN. A more uniform weakly phase separated surface is seen in PP-Tyr/HEMA. The copolymerized PP-Tyr/HEMA film was seen to be defect free with a measured surface microroughness of 0.8 nm, a small increase over that of the pure PP-HEMA film.

dx.doi.org/10.1021/la204416h | Langmuir 2012, 28, 1833−1845

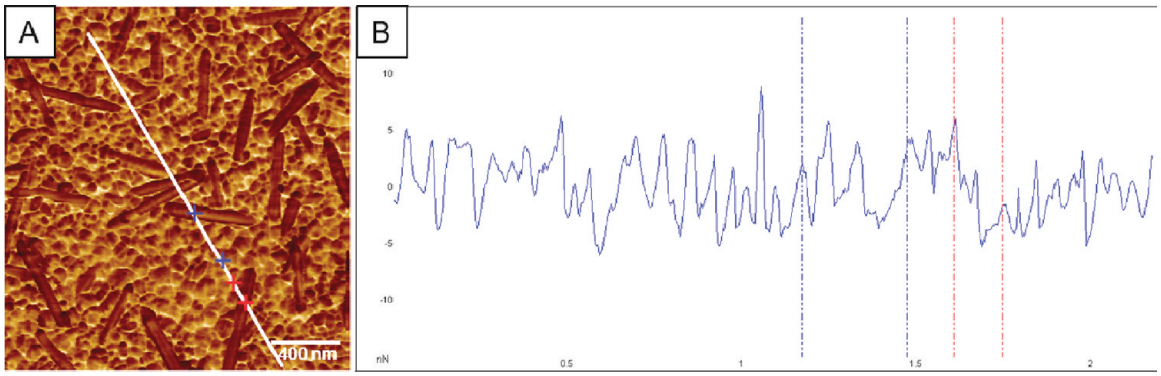

Figure 7. AFM image showing (A) relative adhesion of the PP-Tyr/TTIP needle structures and (B) the topography cross-section (along the white line in (A)) detailing the height and width (nm) of the needles.

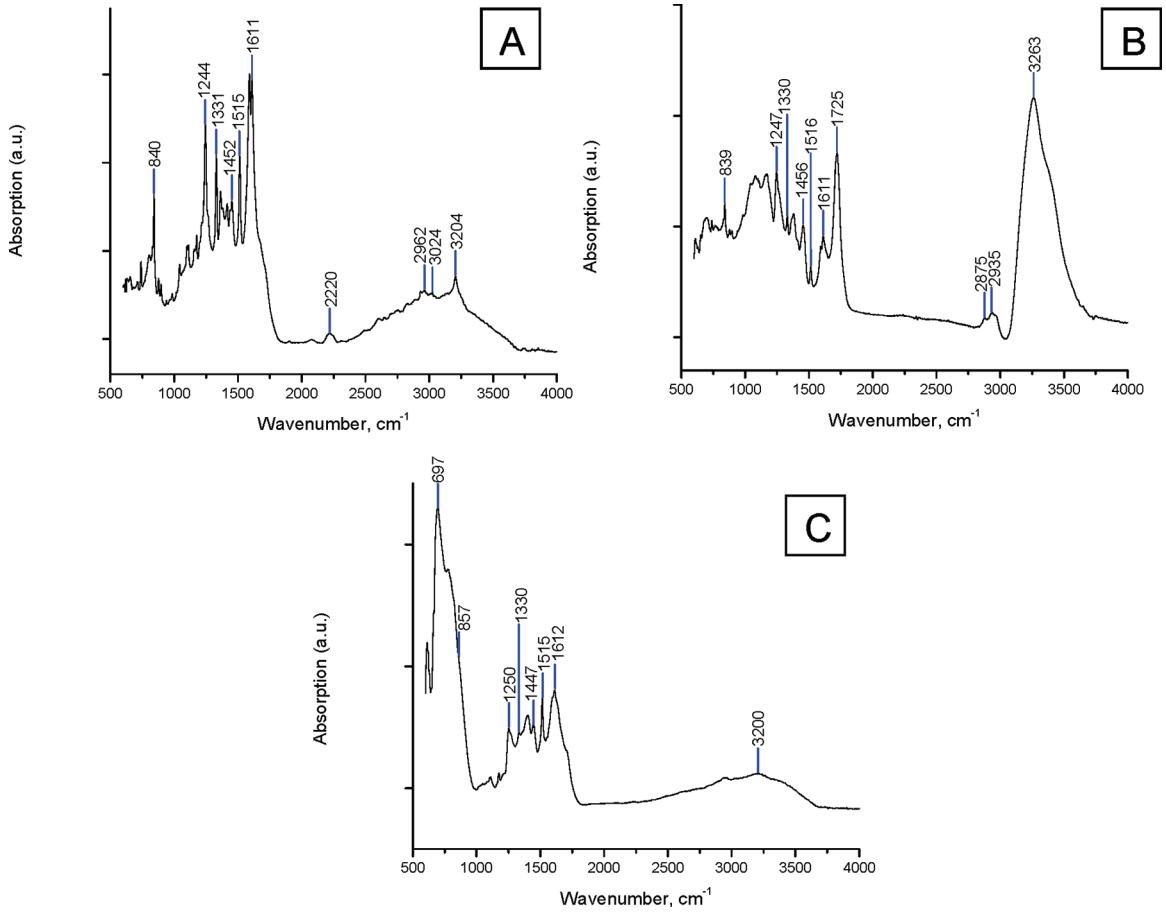

Figure 8. ATR-FTIR spectra of composite coatings: (A) PP-Tyr/ACN, (B) PP-Tyr/HEMA, (C) PP-Tyr/TTIP.

The final copolymerization study utilizing a liquid inorganic component, titanium isopropoxide, and solid L-tyrosine was conducted with the two monomers being vaporized and exposed to the plasma simultaneously. Titanium isopropoxide was heated in a liquid state to facilitate vaporization, while L-tyrosine was sublimed in the same manner used for the single-monomer depositions. The combination of these two materials showed a highly unique microstructure consisting of large needle-like structures embedded in a uniform matrix, which has not been observed in any of our previous plasma deposition studies (Figures 5C and 6C). These needle-like structures are prominently visible in the adhesion variation and are typically measured to be 200−600 nm in length and 20−25 nm in height as can be concluded from AFM cross-section images (Figure 7). We suggest that these needle-like structures are composed of PP-Tyr structures which have grown to larger sizes as compared to the nanoscale features seen on the PP-Tyr film and reported in the literature.[70,71] These studies suggest the formation of tubular structures based upon tyrosine is possible under vacuum deposition conditions and a similar phenomenon may be occurring in our plasma deposition process.[72] These structures are likely seen on the surface of the film as sublimation will continue for a short time after the heating crucible and plasma are switched off while the crucible cools. Tubular structures from amino acids are well documented under this type of physical vapor deposition and will cover the

dx.doi.org/10.1021/la204416h | *Langmuir* 2012, 28, 1833−1845

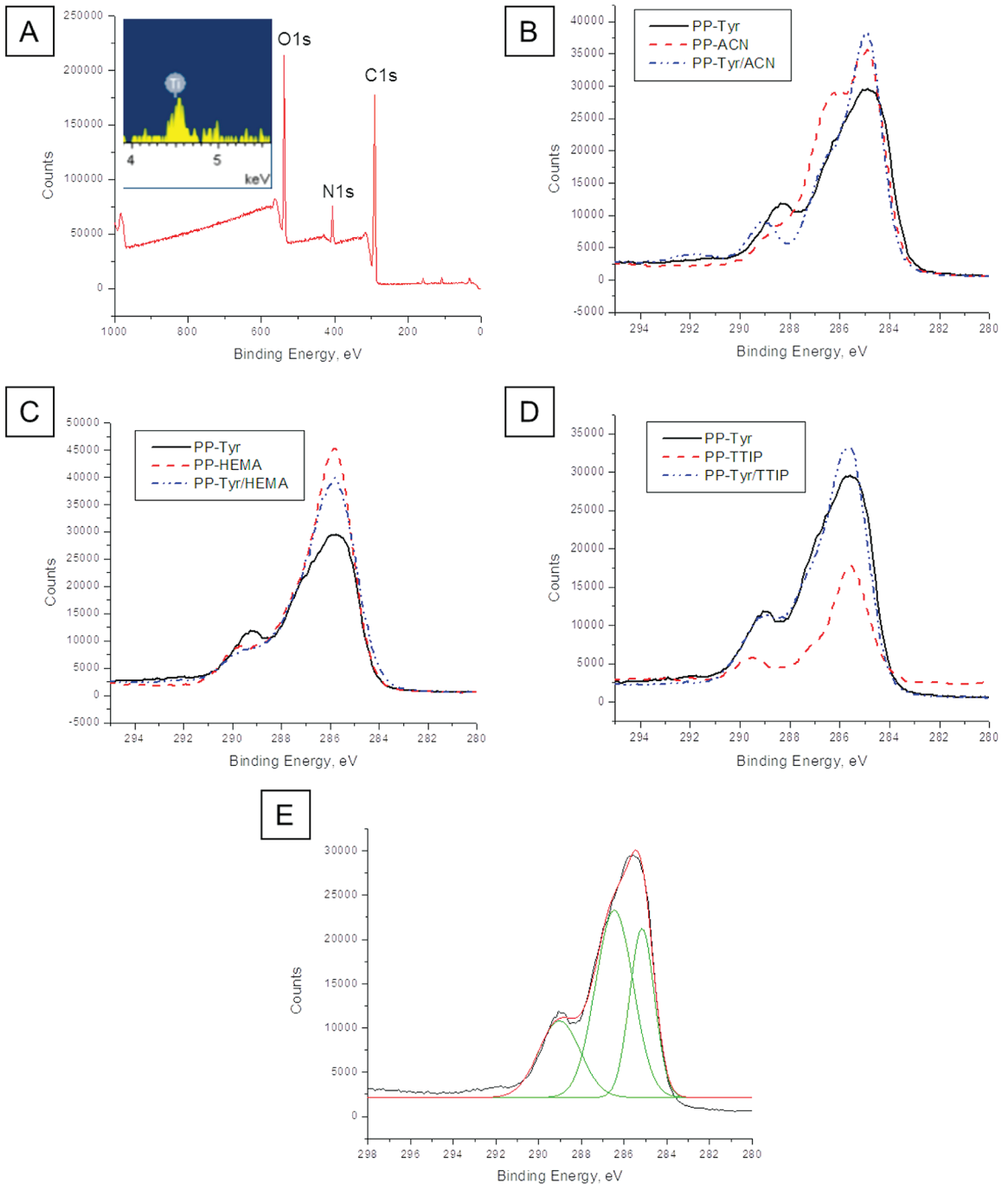

Figure 9. XPS of composite coatings: (A) PP-Tyr/TTIP (inset, EDS spectrum). High-resolution XPS scan of the carbon region: (B) PP-Tyr and PP-ACN, (C) PP-Tyr and PP-HEMA, (D) PP-Tyr and PP-TTIP. (E) Representative plot showing peak deconvolutions of the PP-Tyr film.

surface with pure tyrosine, masking the titanium signal when evaluated via XPS. Any large-scale or repeated microphase separation in the system is unlikely due to the rapid step growth mechanisms of film formation in PECVD. When radicalized species react, they will tend to do so randomly. Local inhomogeneities may well exist in the film as the plasma deposition process is subject to a degree of monomer mixing and randomness during the deposition and a truly homogeneous film would require perfect distribution of the vaporized monomers. Additionally, some radicals go unreacted and are held in place through the cross-linked network which is formed and do not permeate from the film. This would imply that any phase separation occurring after the deposition is unlikely.

In fact, these needle-like structures are dramatically different in comparison to the reported titania structures deposited under oxygen at 298 K.[61] Previous studies have shown titania structures with the round and pitted features seen on our films by AFM (Figure 2 D). No needle-like, lateral features across the top of the film were reported; only vertical features running though the depth of the deposited layer were of prominence. In addition, the surface stiffness map shows little to no relative change in the mechanical properties of the features (Figure 6C). This is an indication that while features are forming in the film during the deposition, they are of a homogenized composition, and no stiffness contrast is observed as would be expected for titania-based structures. Also, needle-like

dx.doi.org/10.1021/la204416h | *Langmuir* 2012, 28, 1833−1845

structures show low adhesion when compared to the rest of the surface, which should be expected for the crystal surface in comparison with the disorganized surrounding surface (Figure 7A). Finally, the absence of a clear titanium signal in the XPS scan sensitive to the topmost 10 nm indicates that the upper surface structures cannot be composed of TTIP monomers (see below).

Chemical Composition of Composite Films: FTIR, XPS, and Spectroscopic Ellipsometry. Common characteristic peaks on FTIR spectra are seen for the composite films and the single material films (Table 1, Figure 8). PP-Tyr/ACN showed major absorption peaks from each monomer, including the C≡N stretch of the cyano group seen near 2220 cm^{-1} and the broad O−H peak of tyrosine centered near 3200 cm^{-1} combined with broad amine peaks and C−H peaks near 3000 and 2960 cm^{-1}.[41,66] Additional peaks correspond well with the remaining PP-Tyr peaks seen in the single-material film, especially those of the aromatic ring at 1611 and 1515 cm^{-1}. The C═N stretch seen in the PP-ACN film is still present near 1675 cm^{-1}, but is convoluted with the aromatic ring peak of PP-Tyr and not readily visible. The PP-Tyr/HEMA composite film shows all of the characteristic FTIR peaks of the PP-Tyr film in addition to the C═O stretch seen in PP-HEMA at 1725 cm^{-1}, which not seen in the PP-Tyr film.

Peaks were also seen near 1160 cm^{-1} indicating C−O bonding and 1079 and 1037 cm^{-1} for C−O−C asymmetric and symmetric vibrations as well as near 1247 cm^{-1} for characteristic amide bonding. Previous studies of tyrosine/HEMA conjugations have reported radicalization of the −OH group on the tyrosine via peroxide exposure, which served as an attachment site for HEMA, and show bonding characteristics similar to those observed here.[48] This study was carried out on tyrosine exposed on a collagen surface and directly modified through peroxide exposure and surface radicalization to bond to free HEMA monomer. The PP-Tyr/TTIP film is seen to retain the Ti−O peak at 697 cm^{-1}, indicating the presence of titania if the total thickness of the film is probed. This peak is shifted and somewhat obscured from Si−C bonding occurring as the deposited material bonds to the surface.

All of the copolymerized films show peaks that are consistent with both the tyrosine ring structure remaining intact and the selected marker peaks from the second component, indicating that copolymerization is occurring and resulting in a highly cross-linked film with a binary composition. This shift from the L-tyrosine position of 876 cm^{-1} is seen in all the composite films at 840, 839, and 857 cm^{-1} for PP-Tyr/ACN, PP-Tyr/HEMA, and PP-Tyr/TTIP, respectively. The PP-Tyr/TTIP peak at 857 cm^{-1} is determined through deconvolution of a single larger peak seen and represents our best estimate. All the peak shifts of this NH_2 peak in the copolymerized films are less than that of L-tyrosine to PP-Tyr, which indicates that the monomers are forming bonds near this position in the molecular structures. The shift shows that this is occurring between the two monomers and they are not solely polymerizing as isolated monomers. It is noted that this NH_2 peak does not appear in the PP-ACN film and is a characteristic peak of tyrosine. These results indicate the presence of tyrosine, and the consistent shift seen in the copolymerized films likely results from NH_2 acting as a bonding site, leading to the conclusion that true copolymerization of the monomers is occurring during the plasma deposition.

XPS of the copolymerized films shows the expected characteristic peaks of PP-Tyr/ACN, PP-Tyr/HEMA, and PP-Tyr/TTIP with strong peaks of carbon, nitrogen, and oxygen as demonstrated in a representative observational XPS plot (Figure 9A). The atomic percentage distributions show the expected elemental presence in the films and generally correspond with the theoretical predictions of the composition (Table 2). The theoretical atomic percentages were estimated assuming a 1:1 ratio of the mixed monomers. While PP-Tyr/ACN and PP-Tyr/TTIP have values that are in general agreement with the expected values for a 1:1 mixture, PP-Tyr/HEMA shows an increased carbon (and thus decreased oxygen) content in the copolymerized film similar to that in the homogeneous PP-HEMA film. The expected nitrogen signal from tyrosine is present in the PP-Tyr/HEMA film but not in the PP-HEMA film, which indicates the presence of both monomers in the PP-Tyr/HEMA film. The excess carbon is likely carbon contamination which commonly occurs on a surface of active plasma-polymerized films.

High-resolution XPS spectra of the carbon content in the PP-Tyr/ACN and the PP-Tyr/HEMA films show a shift of the carbon peaks consistent with combining the two monomers (Figure 9B,C). The primary peaks corresponding to C−C and C−H bonds are present in all single-material films. Deconvolution of all carbon peaks was performed to determine the exact position of all peaks (see the example in Figure 9 E). The PP-Tyr/ACN film shows C═O bonds (289.1 eV) not present in the PP-ACN film and a diluted presence of C−N (286.3 eV) with the addition of the C−C (284.5 eV) bonds from tyrosine.[73] The same C═O shoulder is seen in the PP-HEMA films (289.6 eV) as well and is expected on the basis of its chemical structure. The PP-Tyr/TTIP XPS spectrum shows clear C−C, C−H (285.6 eV), and C−O (289.0 eV) peaks with a broadening of the primary peak from the addition of C−N (287.1 eV) containing tyrosine (Figure 9D). These results indicate that the original molecular carbon architecture remains mainly intact during the plasma polymerization.

The PP-Tyr/TTIP XPS scan shows the carbon, oxygen, and nitrogen peaks as expected, but does not show a clear signature of titanium. We suggest that this result indicates that the titania is buried in the film and is not present at the surface. As known, a common XPS probing depth is around 10 nm for carbon-based materials.[74] A titanium signal is clearly seen, however, at around 4.5 keV in the EDS spectrum (Figure 9A, inset). Additional evidence of the presence of titanium is seen in both FTIR and ellipsometry data. While the amount of titanium seen via EDS is relatively small (∼2 atom %), it confirms the presence of this element in the film, an indication that the copolymerizations are occurring as described and corroborating the FTIR and ellipsometry assertions that titanium is present in the films. The fact that a titanium presence is visible with EDS and FTIR is due to the fact that these techniques probe the composition of the entire film.

As observed, the refractive indices of mixed films fall between the two indices for the individual components as usually observed for mixed films without significant heterogeneities (Figure 10).[39,75] This refractive index can be adjusted depending on the composition of the films by controlling the feed rates of the monomers into the plasma, although this is somewhat more of a challenge to control with a sublimation process. The possibility of the refractive index changing is highlighted in three different examples for the PP-Tyr/HEMA composite film, which shows a lower refractive index after the HEMA supply is increased (Figure 10B). The PP-Tyr/TTIP film clearly shows a higher refractive index than the PP-Tyr

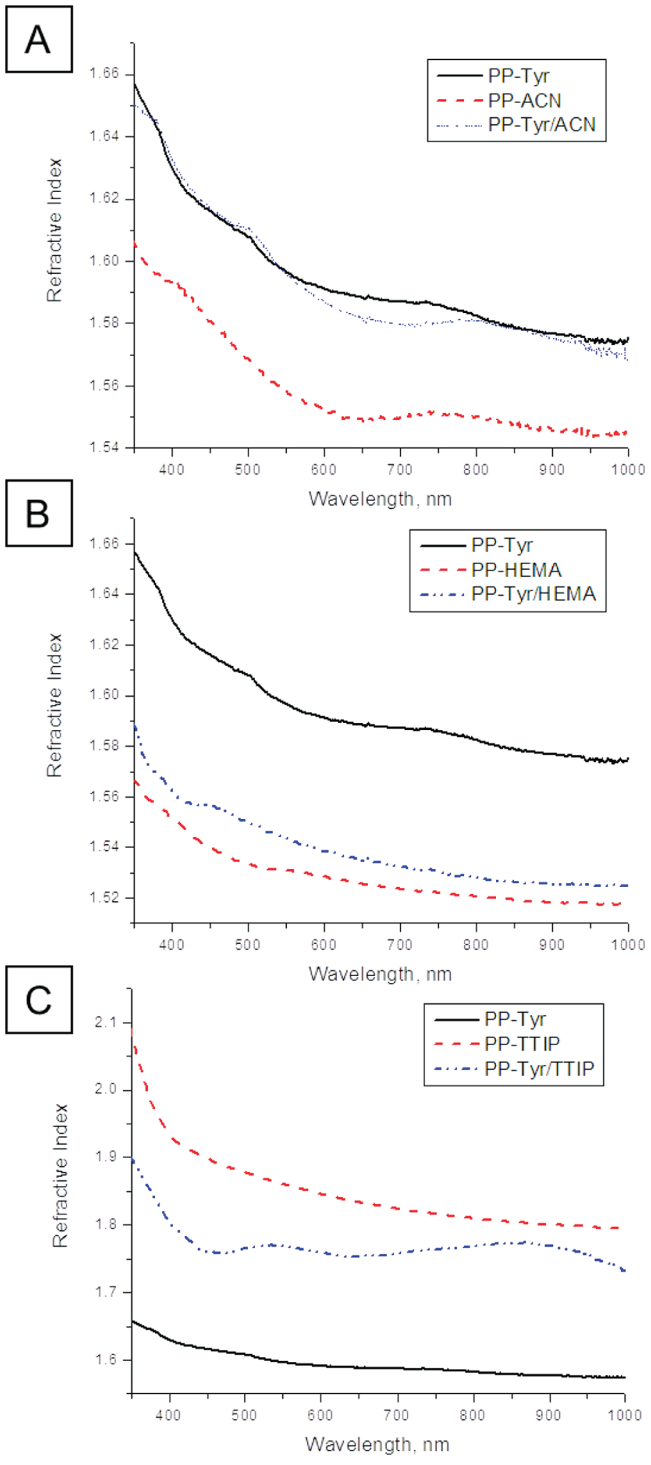

Figure 10. Refractive index of (A) PP-Tyr/ACN, (B) PP-Tyr/HEMA, and (C) PP-Tyr/TTIP coatings.

film, but lower than that of the PP-TTIP film (Figure 10C). The change in refractive index to a higher value is a strong indication of the presence of titania and its role as an optical modifier of the films. It is worth noting that refractive index variation is an important feature which can be adapted to many other plasma-deposited systems as well. Finally, all composite films exhibited a low absorption (k) value of less than 0.04 over the visible spectra, indicating a relatively low light absorption, important for optical coatings.

While these data offer glimpses into the composition and structure of the films, they are not the basis for a final conclusion of the film structure. Further detailed chemical analysis to precisely determine the structure of the plasma-polymerized film could be done via techniques such as NMR and mass spectrometryy. This approach, however, has proven difficult for any polymerized ultrathin coatings (e.g., brushes) due to the insolubility of these coatings.

CONCLUSIONS

We have demonstrated that a selected amino acid, L-tyrosine, is able to be copolymerized with other synthetic organic and inorganic monomers via PECVD to form a stable and robust partially cross-linked composite coating with fine morphology formed by microphase-separated individual components which to great extent preserve their individual chemical composition and morphological features. Copolymerization of materials via sublimation PECVD demonstrates the ability to combine biologic and nonbiologic molecules into a single uniform coating of several hundred nanometers thickness in a rapid, facile, solventless, one-step procedure. This copolymerization method can be used to form biologically active and biofunctionalized robust coatings by adding amino acids and short peptides for organic and inorganic matrixes. We believe that the amino acid used in this study can serve as a proxy for other biological molecules (such as short-chain peptides) which can potentially be copolymerized in a similar fashion with other polymers and inorganic materials to produce robust films with desired compositions and enhanced surface functionality and compatibility. Since the plasma polymerization fabrication approach can be widely applied to many different surfaces, this technique has the potential to be applicable for designing enhanced biological interfaces.

AUTHOR INFORMATION

Corresponding Author

*E-mail: vladimir@mse.gatech.edu.

ACKNOWLEDGMENTS

This work was supported by the Department of Defense (DoD) through the National Defense Science & Engineering Graduate Fellowship (NDSEG) program. This research is also supported by the Air Force Office of Scientific Research (Grants FA9550-08-1-0446 and FA9550-09-1-0162), as well as the Air Force Research Laboratory. We also thank R. Blake Weber for technical assistance.

REFERENCES

(1) Sreenivasan, R.; Gleason, K. K. *Chem. Vap. Deposition* **2009**, *15*, 77−90.
(2) Alf, M. E.; Asatekin, A.; Barr, M. C.; Baxamusa, S. H.; Chelawat, H.; Ozaydin-Ince, G.; Petruczok, C. D.; Sreenivasan, R.; Tenhaeff, W. E.; Trujillo, N. J.; Vaddiraju, S.; Xu, J.; Gleason, K. K. *Adv. Mater.* **2010**, *22*, 1993−2027.
(3) Förch, R.; Chifen, A. N.; Bousquet, A.; Khor, H. L.; Jungblut, M.; Chu, L.-Q.; Zhang, Z.; Osey-Mensah, I.; Sinner, E.-K.; Knoll, W. *Chem. Vap. Deposition* **2007**, *13*, 280−294.
(4) Biederman, H. D. In *Plasma Polymer Films*; Biederman, H., Ed.; Imperial College Press: London, 2004; p 13.
(5) Kuzuya, M.; Noguchi, A.; Ito, H.; Kondo, S.-I.; Noda, N. *J. Polym. Sci., Part A: Polym. Chem.* **1991**, *29*, 1−7.
(6) Hess, D. W. *J. Vac. Sci. Technol., A* **1990**, *8*, 1677−1684.
(7) Tenhaeff, W. E.; Gleason, K. K. *Adv. Funct. Mater.* **2008**, *18*, 979−992.

(8) Friedrich, J.; Kühn, G.; Mix, R. In *Plasma Processes and Polymers*; d'Agostino, R., Favia, P., Oehr, C., Wertheimer, M. R., Eds.; Wiley-VCH Verlag GmbH & Co. KGaA: Weinheim, Germany, 2005; p 10.
(9) Yasuda, H. *Plasma Polymerization*; Academic Press Inc.: New York, 1985; p 6.
(10) Im, S. G.; Gleason, K. K. *AIChE J.* **2011**, *57*, 276−285.
(11) Lau, K. K. S.; Mao, Y.; Lewis, H. G. P.; Murthy, S. K.; Olsen, B. D.; Loo, L. S.; Gleason, K. K. *Thin Solid Films* **2006**, *501*, 211−215.
(12) Karaman, M.; Kooi, S. E.; Gleason, K. K. *Chem. Mater.* **2008**, *20*, 2262−2267.
(13) Choukourov, A.; Biederman, H.; Slavinska, D.; Hanley, L.; Grinevich, A.; Boldyryeva, H.; Mackova, A. *J. Phys. Chem. B* **2005**, *109*, 23086−23095.
(14) Tamirisa, P. A.; Koskinen, J.; Hess, D. W. *Thin Solid Films* **2006**, *515*, 2618−2624.
(15) Tamirisa, P. T.; Hess, D. W. *Macromolecules* **2006**, *39*, 7092−9097.
(16) Chan, K.; Gleason, K. K. *Langmuir* **2005**, *21*, 8930−8939.
(17) López, G. P.; Ratner, B. D. *J. Polym. Sci., Part A: Polym. Chem.* **1992**, *30*, 2415−2425.
(18) Anderson, K. D.; Slocik, J. M.; McConney, M. E.; Enlow, J. O.; Jakubiak, R.; Bunning, T. J.; Naik, R. R.; Tsukruk, V. V. *Small* **2009**, *5*, 741−749.
(19) Anderson, K. D.; Marczewski, K.; Singamaneni, S.; Slocik, J. M.; Naik, R. R.; Bunning, T. J.; Tsukruk, V. V. *Appl. Mater. Int.* **2010**, *2*, 2269−2281.
(20) Anderson, K. D.; Luo, M.; Jakubiak, R.; Naik, R. R.; Bunning, T. J.; Tsukruk, V. V. *Chem. Mater.* **2010**, *22*, 3259−3264.
(21) Khan, H. U.; Roberts, M. E.; Johnson, O.; Förch, R.; Knoll, W.; Bao, Z. *Adv. Mater.* **2010**, *22*, 4452−4456.
(22) Singamaneni, S.; McConney, M. E.; Tsukruk, V. V. *Adv. Mater.* **2010**, *22*, 1263−1268.
(23) LeMieux, M. C.; McConney, M. E.; Lin, Y.-H.; Singamaneni, S.; Jiang, H.; Bunning, T. J.; Tsukruk, V. V. *Nano Lett.* **2006**, *6*, 730−734.
(24) Singamaneni, S.; LeMieux, M. C.; Lang, H. P.; Gerber, C.; Lam, Y.; Zauscher, S.; Datskos, P. G.; Lavrik, N. V.; Jiang, H.; Naik, R. R.; Bunning, T. J.; Tsukruk, V. V. *Adv. Mater.* **2008**, *20*, 653−680.
(25) Pan, Y. V.; Wesley, R. A.; Luginbuhl, R.; Denton, D. D.; Ratner, B. D. *Biomacromolecules* **2001**, *2*, 32−36.
(26) Johnson, E. M.; Clarson, S. J.; Jiang, H.; Su, W.; Grant, J. T.; Bunning, T. J. *Polymer* **2001**, *42*, 7215−7219.
(27) Lahann, J. *Polym. Int.* **2006**, *55*, 1361−1370.
(28) Chen, H.-Y.; Lahann, J. *Langmuir* **2011**, *27*, 34−48.
(29) Slocik, J. M.; Beckel, E. R.; Jiang, H.; Enlow, J. O.; Zabinski, J. S. Jr.; Bunning, T. J.; Naik, R. R. *Adv. Mater.* **2006**, *18*, 2095−2100.
(30) Lee, N. H.; Frank, C. W. *Langmuir* **2003**, *19*, 1295−1303.
(31) Mari-Buye, N.; O'shaughnessy, S.; Colominas, C.; Semino, C. E.; Gleason, K. K.; Borros, S. *Adv. Funct. Mater.* **2009**, *19*, 1276−1286.
(32) Enlow, J. O.; Jiang, H.; Grant, J. T.; Eyink, K.; Su, W.; Bunning, T. J. *Polymer* **2008**, *49*, 4042−4045.
(33) Aparicio, F. J.; Holgado, M.; Borras, A.; Blaszczyk-Lezak, I.; Griol, A.; Barrios, C. A.; Casquel, R.; Sanza, F. J.; Sohlström, H.; Antelius, M.; González-Elipe, A. R.; Barranco, A. *Adv. Mater.* **2011**, *23*, 761−765.
(34) Aparicio, F. J.; Borras, A.; Blaszczyk-Lezak, I.; Gröning, P.; Álvarez-Herrero, A.; Fernández-Rodríguez, M.; González-Elipe, A. R.; Barranco, A. *Plasma Processes Polym.* **2009**, *6*, 17−26.
(35) Blaszczyk-Lezak, I.; Aparicio, F. J.; Borrás, A.; Barranco, A.; Álvarez-Herrero, A.; Fernández-Rodríguez, M.; González-Elipe, A. R. *J. Phys. Chem. C* **2009**, *113*, 431−438.
(36) Barranco, A.; Groening, P. *Langmuir* **2006**, *22*, 6719−6722.
(37) Singamaneni, S.; Kharlampieva, E.; Jang, J. H.; McConney, M. E.; Jiang, H.; Bunning, T. J.; Thomas, E. L.; Tsukruk, V. V. *Adv. Mater.* **2010**, *22*, 1369−1373.
(38) Dickerson, M. B.; Sandhage, K. H.; Naik, R. R. *Chem. Rev.* **2008**, *108*, 4935−4978.
(39) Jiang, H.; O'Neill, K.; Grant, J. T.; Tullis, S.; Eyink, K.; Johnson, W. E.; Fleitz, P.; Bunning, T. J. *Chem. Mater.* **2004**, *16*, 1292−1297.
(40) Jiang, H.; Eyink, K.; Grant, J. T.; Enlow, J.; Tullis, S.; Bunning, T. J. *Chem. Vap. Deposition* **2008**, *14*, 286−291.
(41) Singamaneni, S.; LeMieux, M. C.; Jiang, H.; Bunning, T. J.; Tsukruk, V. V. *Chem. Mater.* **2007**, *19*, 129−131.
(42) Singamaneni, S.; McConney, M. E.; LeMieux, M. C.; Jian, H.; Enlow, J. O.; Bunning, T. J.; Naik, R. R.; Tsukruk, V. V. *Adv. Mater.* **2007**, *19*, 4248−4255.
(43) Wichterle, O.; Lim, D. *Nature* **1960**, *165*, 117−118.
(44) Jeyanthi, R.; Rao, K. P. *Biomaterials* **1990**, *11*, 238−243.
(45) Pfluger, C. A.; Carrier, R. L.; Sun, B.; Ziemer, K. S.; Burkey, D. D. *Macromol. Rapid Commun.* **2009**, *30*, 126−132.
(46) Bose, R. K.; Lau, K. K. S. *Biomacromolecules* **2010**, *11*, 2116−2122.
(47) Quinn, C. P.; Pathak, C. P.; Heller, A.; Hubbell, J. A. *Biomaterials* **1995**, *16*, 389−396.
(48) Wang, D.; Williams, C. G.; Yang, F.; Elisseeff, J. H. *Adv. Funct. Mater.* **2004**, *14*, 1152−1159.
(49) Tsukruk, V. V.; Bliznyuk, V. N. *Langmuir* **1998**, *14*, 446−455.
(50) Haaland, P.; Targove, J. *Appl. Phys. Lett.* **1992**, *61*, 34−36.
(51) Jiang, H.; Johnson, W. E.; Grant, J. T.; Eyink, K.; Johnson, E. M; Tomlin, D. W.; Bunning, T. J. *Chem. Mater.* **2003**, *15*, 340−347.
(52) Jiang, H.; Hong, L.; Venkatasubramanian, N.; Grant, J. T.; Eyink, K.; Wiacek, K.; Fries-Carr, S.; Enlow, J.; Bunning, T. J. *Thin Solid Films* **2007**, *515*, 3513−3520.
(53) Jiang, H.; Grant, J. T.; Eyink, K.; Tullis, S.; Enlow, J.; Bunning, T. J. *Polymer* **2005**, *46*, 8178−8184.
(54) Peri, S. R.; Habersberger, B.; Akgun, B.; Jiang, H.; Enlow, J.; Bunning, T. J.; Majkrzak, C. F.; Foster, M. D. *Polymer* **2010**, *51*, 4390−4397.
(55) McConney, M. E.; Singamaneni, S.; Tsukruk, V. V. *Polym. Rev.* **2010**, *50*, 235−286.
(56) Pashley, M. D. *Colloids Surf.* **1984**, *12*, 69−77.
(57) Piétrement, O.; Troyon, M. *J. Colloid Interface Sci.* **2000**, *226*, 166−171.
(58) Kharlampieva, E.; Slocik, J. M.; Singamaneni, S.; Poulsen, N.; Kroger, N.; Naik, R. R.; Tsukruk, V. V. *Adv. Funct. Mater.* **2009**, *19*, 2303−2311.
(59) Choi, I.; Suntivich, R.; Plamper, F. A.; Synatschke, C. V.; Müller, A. H. E.; Tsukruk, V. V. *J. Am. Chem. Soc.* **2011**, *133*, 9592−9606.
(60) Peri, S. R.; Kim, H.; Akgun, B.; Enlow, J.; Jiang, H.; Bunning, T. J.; Li, X.; Foster, M. D. *Polymer* **2010**, *51*, 3971−3977.
(61) Borras, A.; Cotrino, J.; González-Elipe, A. R. *J. Electrochem. Soc.* **2007**, *154*, 152−157.
(62) Alvarez, R.; Romero-Gomez, P.; Gil-Rostra, J.; Cotrino, J.; Yubero, F.; Palmero, A.; González-Elipe, A. R *J. Appl. Phys.* **2010**, *108*, 064316.
(63) Ahn, K.-H.; Park, Y.-B.; Park, D.-W. *Surf. Coat. Technol.* **2003**, *171*, 198−204.
(64) Jiang, H.; Grant, J. T.; Enlow, J.; Su, W.; Bunning, T. J. *J. Mater. Chem.* **2009**, *19*, 2234−2239.
(65) Sweers, K.; van der Werf, K.; Bennink, M.; Subramaniam, V. *Nanoscale Res. Lett.* **2011**, *6*, 270.
(66) Grace, L. I.; Cohen, R.; Dunn, T. M.; Lubman, D. M.; de Vries, M. S. *J. Mol. Spectrosc.* **2002**, *215*, 204−219.
(67) Hernandez-Perez, M. A.; Garapon, C.; Champeaux, C.; Orlianges, J. C. *J. Phys: Conf. Ser.* **2007**, *59*, 724−727.
(68) Tarducci, C.; Schofield, W. C. E.; Badyal, J. P. S; Brewer, S. A.; Willis, C. *Chem. Mater.* **2002**, *14*, 2541−2545.
(69) Fictorie, C. P.; Evans, J. F.; Gladfelter, W. L. *J. Vac. Sci. Technol., A* **1994**, *12*, 1108−1113.
(70) Spear, R. L.; Tamayev, R.; Fath, K. R.; Banerjee, I. A. *Colloids Surf., B* **2007**, *60*, 158−166.
(71) Reches, M.; Gazit, E. *Nat. Nanotechnol.* **2006**, *1*, 195−200.
(72) Adler-Abramovich, L.; Aronov, D.; Beker, P.; Yevnin, M.; Stempler, S.; Buzhansky, L.; Rosenman, G.; Gazit, E. *Nat. Nanotechnol.* **2009**, *4*, 849−854.
(73) Tsukruk, V. V.; Luzinov, I.; Julthongpiput, D. *Langmuir* **1999**, *15*, 3029−3032.

(74) Luzinov, I.; Julthongpiput, D.; Liebmann-Vinson, A.; Cregger, T.; Foster, M. D.; Tsukruk, V. V. *Langmuir* **2000**, *16*, 504−516.
(75) Grant, J. T.; Jiang, H.; Tullis, S.; Johnson, W. E.; Eyink, K.; Fleitz, P.; Bunning, T. J. *Vacuum* **2005**, *80*, 12−19.